Effect of Arc Force on Defect Formation in GTA Welding

Increasing welding speed beyond a critical limit results in weld-bead undercutting and/or humping which are related to arc force and its distribution

BY W. F. SAVAGE, E. F. NIPPES AND K. AGUSA

ABSTRACT. This investigation deals with the mechanism of formation of defects in GTA welding. Increasing the welding speed beyond a critical limit results in deterioration of the weld bead by undercutting and/or humping. The travel-speed limit was observed to increase with the use of:

1. Lower welding current.
2. He shielding gas.
3. Shorter electrode-to-work distance.
4. Smaller diameter electrodes.
5. Larger included angles at the apex of the conical tip of the electrode.
6. Lower frequency pulsed-current.

An arc-force measurement system, utilizing a linear variable differential transformer, was effective for measuring the total arc force which acts against a plate surface during welding. The arc force was found to be a function of both electrode-to-work distance and welding current and was not affected by travel speed, shielding gas, electrode geometry, or pulse frequency. When the electrode-to-work distance was held constant at 2.4 mm (0.094 in.), the arc force varied linearly from 2.6 to 14.3 grams for welding currents of 100 to 550 amperes. This linear relationship existed between welding current and arc force, regardless of whether weld defects were present or not.

There was no direct relationship between the travel-speed limits and the total arc force. The observations of the bead cross-sections revealed, however, that the welding variables which gave the higher travel-speed limits had a tendency to produce either a concave or flat root penetration. From this fact, the effective arc pressure for the formation of weld defects was considered to be low under those welding variables, even though the total arc force remained the same.

Introduction

This investigation deals with the relationship between arc force and the mechanism of weld-defect formation in gas tungsten arc (GTA) welding. Three types of weld defects are of specific interest:

1. Humping—an irregular surface contour consisting of a series of bead-like protuberances separated by intervals of relatively uniform bead-surface contour.
2. Undercutting—a groove, melted into the base metal adjacent to the fusion zone, which is left unfilled with weld metal.
3. Tunnelling—a special form of undercut in which an open channel, which remains unfilled with weld metal, is formed at the root.

In arc welding, it is well known that increasing the welding speed beyond a certain critical limit results in deterioration of the weld bead in the form of undercutting and/or humping. The prevention or minimization of these defects is a highly important goal, because it would permit increasing the maximum welding speed and, therefore, the melting efficiency. As a first step, it is necessary to clarify the mechanism of formation of these defects.

The main reason for the defects is the time interval between the gouging of a channel on a plate surface by the arc and the filling of this channel with molten metal.[1-4] Under the welding conditions which produce weld defects, the molten metal beneath the arc is forced to move toward the rear of the pool and a gouged solid surface appears beneath the arc. As the arc moves ahead, no defect occurs if the molten metal in the rear of the pool flows forward and fills the entire gouged region. Conversely, either rapid solidification of the molten metal at the rear of the pool or imperfect filling with the molten metal results in the formation of weld defects. Both the physical and metallurgical properties of the gouged surface are important factors affecting defect formation. However, the published literature does not contain much information regarding effects of these properties.[5]

Two factors have been considered to be responsible for the movement of the molten metal and the appearance of the gouged surface. First, the temperature difference between the front and the back of the pool alters the surface tension in such a manner as to cause the molten metal to flow to the rear of the pool.[1] However, quantitative studies of this effect have not been reported. The other reason for the appearance of the gouged surface is the arc pressure which acts on the molten metal at the front of the pool.[1-4] In general, this is considered to be the major factor responsible for the

W. F. SAVAGE is Professor of Metallurgical Engineering and Director of Welding Research; E. F. NIPPES is Professor of Metallurgical Engineering, Rensselaer Polytechnic Institute, Troy, New York; K. AGUSA, former Research Fellow at RPI, is with the Welding Section, Research Laboratories, Kawasaki Steel Corporation, Chiba, Japan.

movement of the molten metal. Super-critical flow has been proposed[3] as an additional factor which may affect the movement of the molten metal. When the thickness of the molten metal in the front of the pool is reduced to a critical value by the arc pressure, the flow rate of the molten metal is accelerated by the super-critical flow phenomenon and the liquid tends to pile up at some point on the flow path.

Three major causes have been reported for the arc force which acts against the plate:[6-10]

1. The electro-magnetic force,
2. The plasma jet force.
3. The electron impingement force.

It is generally believed that the plasma jet is the most powerful component of the arc force.

Object

The major purposes of this investigation were:

1. To analyze the effect of welding variables on the formation of weld defects in GTA welding.
2. To measure the effect of welding variables on the arc force in GTA welding.
3. To discuss the relationship between arc force and weld defect formation in GTA welding.

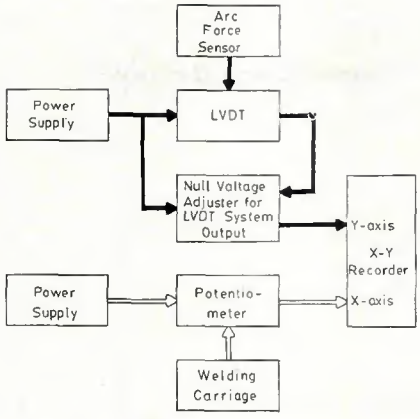

Fig. 1—Block diagram for arc-force measuring equipment

Material

The material used in this investigation was Republic 70 Precipitation Hardening Steel supplied by Republic Steel Corporation in the form of specimens 2 in. (51 mm) wide × 6 in. (152 mm) long × ¾ in. (19 mm) thick. The nominal chemical composition (wt-%) of this material is as follows: C—0.20, Si—0.15, Mn—1.00, P—0.04, S—0.04, Cu—1.00 to 1.50, Mo—0.20 to 0.30, and Ni—1.20 to 1.75.

The ¾ in. (19 mm) plate thickness was chosen to realize three-dimensional heat flow through the specimen. All plates were used in the hot-rolled condition, and the surfaces to be welded were either ground smooth or sand-blasted.

Experimental Procedures

The study consisted of two major portions:

1. The determination of the maximum travel speed which could be used without creating weld defects under different welding conditions (hereafter referred to as the travel-speed limit).
2. The measurement of the influence of welding variables on the total arc force.

The preliminary experiments indicated that to obtain accurate and reproducible travel-speed limits, several arc-on periods are required before data sampling in order to stabilize the surface condition of the as-ground, thoriated-W electrode. Although the reason for this has not been clarified by this investigation, changes in the electrode surface during repeated arc-on periods appear to "condition" the electrode and stabilize the welding arc.

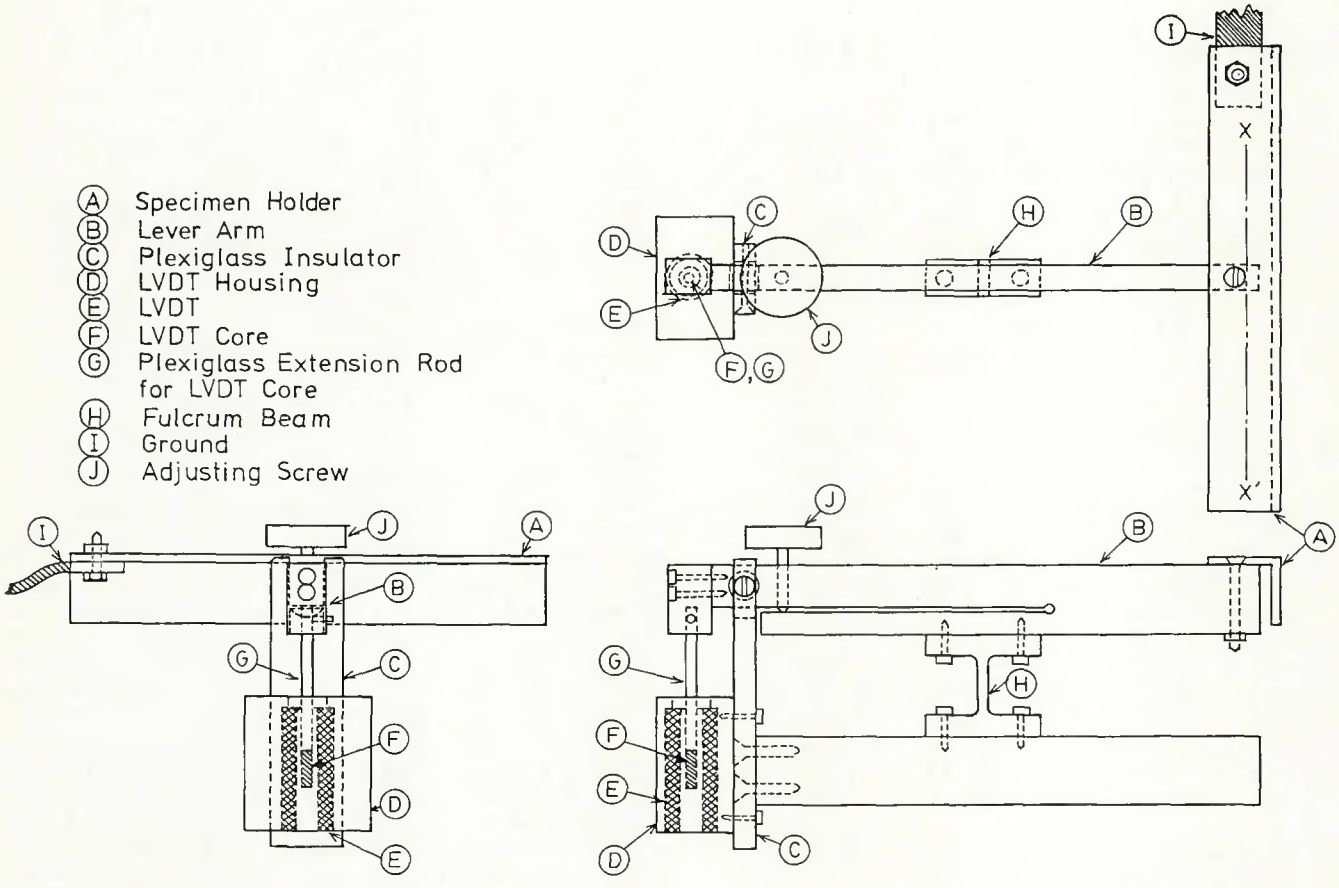

Fig. 2—Detail drawing of arc-force sensing apparatus

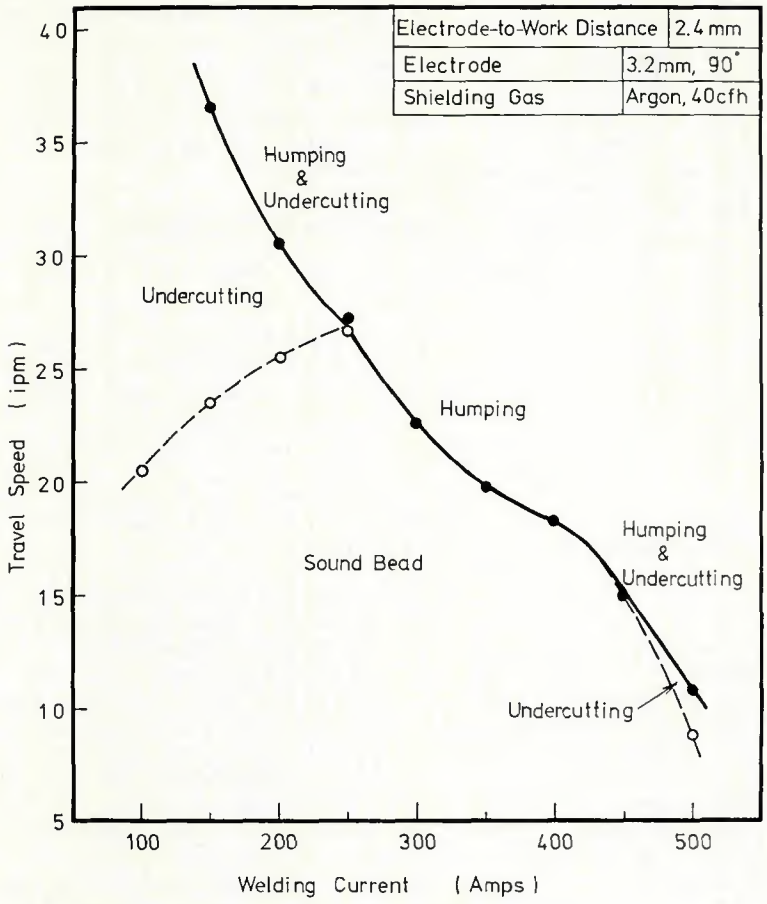

Fig. 3—Effect of welding current on travel-speed limit

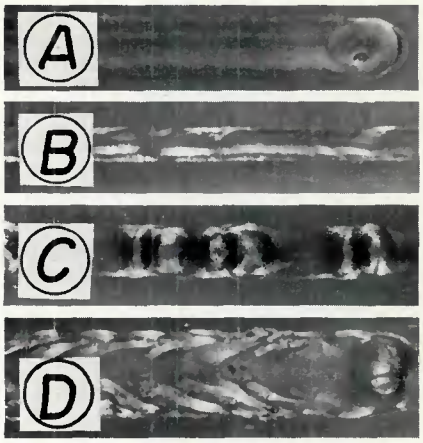

Fig. 4—Typical weld-bead appearance obtained with different welding conditions. Electrode-to-work distance—2.4 mm; electrode—3.2 mm, 90 deg.; shielding gas—argon, 40 cfh

Welding Power Supply

All welds were made with an *Airco Sampac Programmed* GTA welding system. The welding mode was DCSP and the power supply was used in the *constant current* mode. The power supply and travel carriage operate as closed-loop servo systems with the following accuracies: current, ± 6 amperes (A); voltage, ± 0.2 volts (V); and speed, ± 0.1 ipm (0.04 mm/sec).

A low-frequency, square-pulse generator, with a maximum pulse frequency of 4 cps, was used to study the effect of pulsating current on both the travel-speed limit and the arc force. The combination of maximum and minimum current could be chosen between 30 to 600 A without restriction. The arc duration at both maximum and minimum current could be independently controlled within the range from 0.125 to 3.0 seconds (s).

In this investigation, argon (Ar) was used as a shielding gas but, for comparison, helium (He) was also used in selected experiments. Gas flow rate was held constant at 40 cfh (19 liters/min) throughout the investigation.

Centerless-ground, W-2% thoria electrodes were used exclusively. The diameters of electrodes were 1/8, 5/32, and 3/16 in. (3.2, 4.0, and 4.8 mm), with a vertex angle of the conical tip of either 18 or 90 deg. Electrode extension, held constant at 0.20 in. (5.08 mm) measured from the bottom of the gas cup, corresponded to a dimension of 1.043 in. (26.5 mm) from the water-cooled collet.

Welding Procedures

To investigate the influence of arc force on weld-bead formation, it is necessary not only to measure the magnitude of arc force but also to note the deflection of the arc. This is true because the flow pattern in the molten pool is greatly affected by the deflection of the arc. As a result, the formation of the weld bead is greatly influenced by this flow pattern. It is well known that higher travel speeds can be used with a forehand arc angle than with a backhand arc angle. It is to be noted that the forehand arc points in the direction of travel, while the backhand arc points in the opposite direction.

In addition, attention must be paid to the electrode-surface condition. Theoretical analysis[8,9] predicts that the plasma jet should be the most powerful component of the arc pressure. The plasma jet velocity is directly related to the current density which is influenced by the surface condition of the electrode tip.

Preliminary experiments were undertaken to determine the effect of both arc deflection and electrode-surface condition on the formation of the weld bead. The welding procedures used in the balance of the study were based upon the results of these preliminary investigations.

Effect of Arc Deflection. The factors which deflect an arc from a line perpendicular to the plate being welded are:

1. The angle between the electrode and the work.
2. The magnetic arc blow near the edge of the plate.
3. The presence and direction of the residual magnetic field in the plate.
4. The electro-magnetic force caused by the interaction of the arc plasma with current elements within the plate.

Electrodes were maintained perpendicular to the plate surface in all cases. The welds were made well within the edges of the plate so that the effect of magnetic blow at plate edges could be eliminated. Also, to eliminate any residual magnetic field, all plates were thoroughly demagnetized before welding.

The electro-magnetic force caused by the interaction of the plasma with current elements within the plate is inevitable, and the arc deflection caused by this force depends on the ground position. When the ground connection is made at the starting side (Mode A), the arc deflects forward, and when made at the finishing side (Mode C), the arc deflects backward. Weld defects are less likely to occur when the arc is deflected forward. When the ground was attached at

both ends of the plate (Mode B), the arc became essentially perpendicular to the plate surface. However, the arc stability in Mode B was poorer than that in either Mode A or Mode C, because the distribution of the current between the two ground connections is not necessarily equal in Mode B.

In this investigation, Mode A, which permitted the highest travel-speed limit at a given current, was used.

Effect of Electrode-Surface Condition. The effect of the number of arc-on periods on the surface condition of the electrodes was investigated. The relationship between the number of humps formed on 5 in. (127 mm) long beads and the number of times the electrode was used after regrinding the tip was determined. Each arc-on period involved making a bead-on-plate weld with the following conditions: arc current—300 A, travel speed—22.5 ipm (9.64 mm/s), and travel length—5 in. (127 mm).

Five to nine humps were formed per 5 in. (127 mm) length with freshly ground electrodes, and the number of humps decreased to zero after 10 or more arc-on periods.

Although the cause of the phenomenon is not certain, it is probable that the thermionic emission from a thoriated tungsten (W) electrode is affected by the changes in its surface condition produced by the arc-on periods. Consequently, in this investigation, all electrodes were subjected to 10 arc-on times at the current to be used prior to determining the travel-speed limit.

Determination of Travel-Speed Limits. In this investigation, the effects of welding variables on both the travel-speed limit and the arc force were studied. The welding variables investigated included:

1. Welding current (100–550 A).
2. Shielding gas (Ar and He).
3. Electrode-to-work distance (0.04–0.06 in., 1.0–4.0 mm).
4. Electrode diameter (0.125–0.189 in. 3.2–4.8 mm).
5. Vertex angle of electrode tip (18 and 90 deg).
6. Frequency of pulsed-current (0–3.35 cps).

The procedure for determining travel-speed limits under various welding conditions was as follows:

1. For each combination of welding variables to be studied, the thoriated W electrodes were conditioned by making ten 5 in. (127 mm) beads at 20 to 25 ipm (8.47 to 10.6 mm/s) before making the data-sampling run.
2. A travel speed for welding was arbitrarily chosen. If the weld bead obtained did not include any defects, the travel speed was increased until weld defects began to appear. The travel speed was usually increased in increments of 1.0 ipm (0.42 mm/s) except near the travel-speed limit where increments of 0.5 ipm (0.21 mm/s) were used.
3. The travel-speed limit was selected as the mid-point between the two travel speeds which produce the first defective bead and the last sound weld bead. The average error in determining the travel-speed limit was approximately ± 0.25 ipm (± 0.106 mm/s).

Equipment and Procedure for Measuring Arc Force

The main objective of measuring arc force is to evaluate the total force acting against the plate surface during welding. The block diagram in Fig. 1 indicates the major components of the apparatus used to measure the total arc force.

The transducer used is a Schaevitz Engineering Type 050-DC-D Linear Variable Differential Transformer (LVDT) which has a linear transfer function of 200.7 V/in. (7.9 V/mm) over a range of 0.050 in. (1.27 mm).

Figure 2 illustrates the device used to sense the arc force during this investigation. The device, machined from an Al alloy, utilized a plexiglass plate, C, which electrically insulated the LVDT housing, D. The extension rod for the LVDT core, G, was made of plexiglass both to eliminate ferromagnetic effects and to provide electrical insulation between the core and the rest of the device. The ground cable, I, was made of a flexible, flat-woven Cu cable.

Procedure for using the arc-force sensor is summarized below:

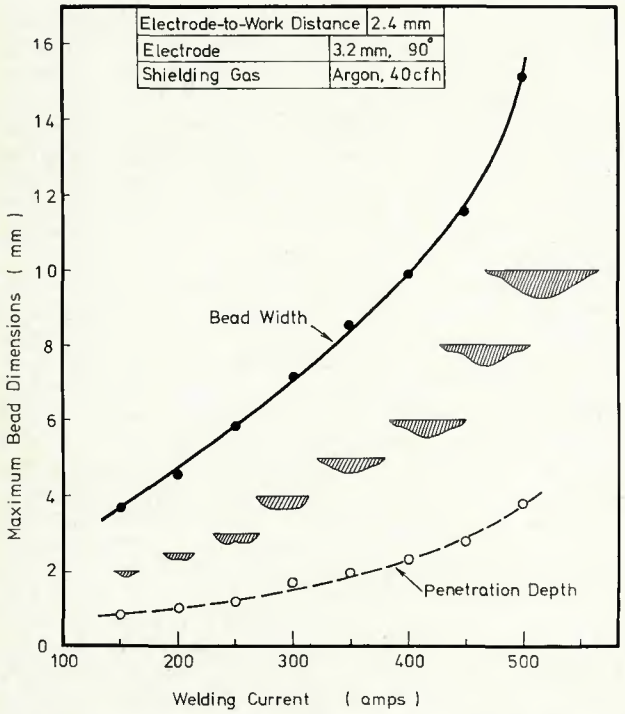

Fig. 5—Maximum dimensions and cross-sections of the weld beads obtained at travel-speed limits

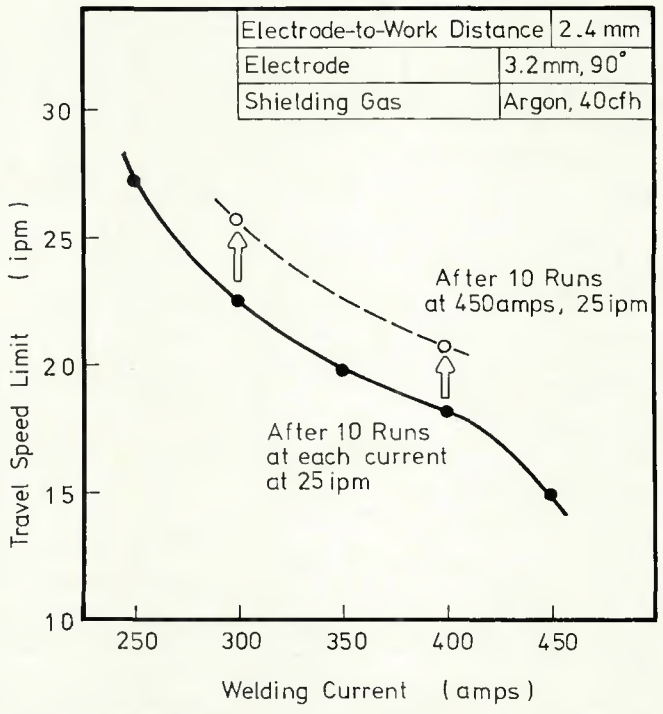

Fig. 6—Effect of electrode-surface condition on travel-speed limit

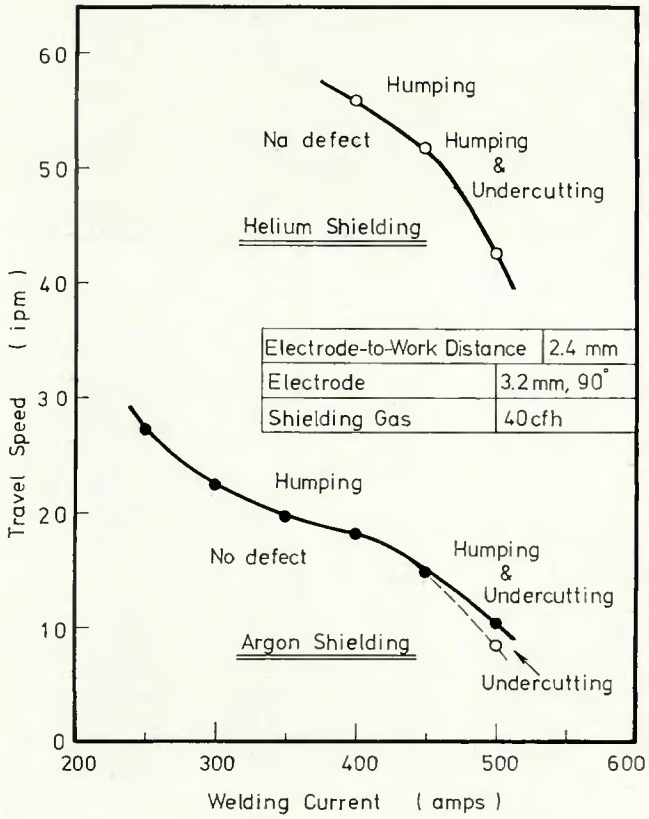

Fig. 7—Effect of shielding gas on travel-speed limit

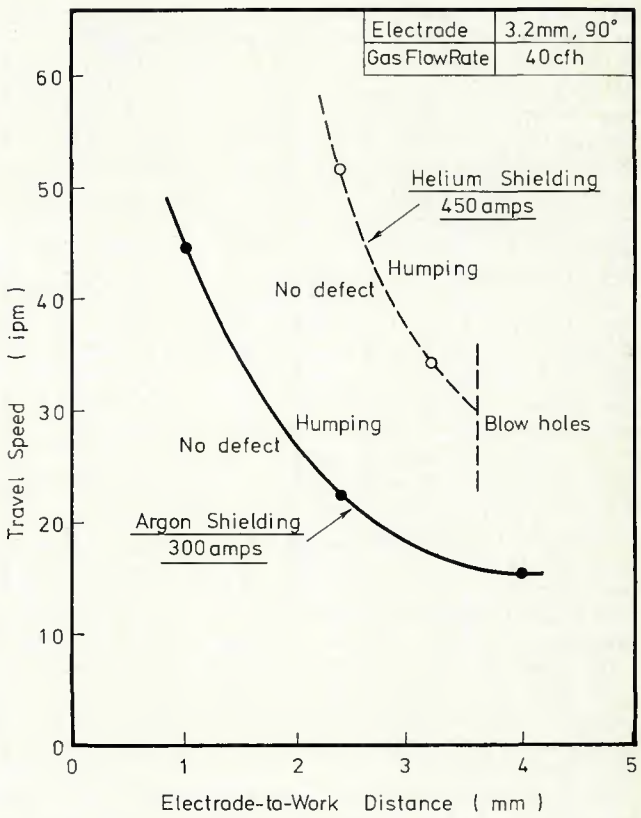

Fig. 8—Effect of electrode-to-work distance on travel-speed limit

1. Adjust the angle of the specimen holder, A, so that it is perpendicular to the lever arm, B. The actual arc-force sensing device had a means for accurately adjusting this angle; to simplify the drawing, however, it is not illustrated.

2. Fix the position of the arc-force sensor so that the W electrode tracks the centerline X-X′ of the specimen holder, A.

3. Mount a specimen on the specimen holder, A, and adjust the output voltage of the LVDT to zero with the null-voltage control in Fig. 1. If the output voltage is outside the range of the null-voltage control, move the LVDT core, F, up or down by rotating the screw, J, until null-voltage is achieved.

4. Initiate the arc with a high-frequency starting current and record the output of the transducer as a function of arc position on an X-Y recorder.

Steps 1 and 2 assured that the effective lever length from a moving arc to the fulcrum beam, H, would be constant.

The arc force measuring system was calibrated by placing different weights on a specimen mounted on the specimen holder. A linear relationship of 0.166 mV/gram was obtained between the output voltage of the LVDT and the load placed on a specimen. No significant difference in the calibration was noted when the position of the weight was varied along the welding axis.

In the course of the arc-force measurements using the LVDT system, special attention was devoted to the fact that any magnetic materials located around the specimen holder could produce errors in the magnitude of the LVDT output. The magnetic fields made by the current through the specimen and its holder are distorted by magnetic materials, and such distorted fields cause deflection of the specimen holder. As an example, a steel plate placed 2.5 in. (63.5 mm) beneath the specimen holder doubled the output of the device for a given welding current. To minimize the magnetic-field effect during actual measurements, the nearest magnetic material to the specimen holder was the track of the welding carriage which was located 16 in. (0.4 m) to the rear of the axis of the weld.

Results and Discussion

Effect of Welding Current

In the relationship between travel-speed limit and the magnitude of welding current, shown in Fig. 3, three welding current ranges can be identified:

Range I—arc currents below 250 A. In this range, undercutting occurred at lower travel speeds than did humping, and the curve of the travel-speed limit for undercutting exhibited a positive slope while that of the travel-speed limit for humping exhibited a negative slope.

Range II—arc currents between 250 and 430 A. In this range, the travel-speed limit was determined by humping alone.

Range III—arc currents above 430A. In this range, undercutting occurred again at lower travel speeds than did humping, and the slope of both travel-speed limit curves became more sharply negative.

Figure 4 shows the typical appearance of weld beads in each region. The undercutting observed in the high-current range has a step pattern on its surface (Fig. 4D) and, thus, differs from the undercutting which occurs in the low-current range (Fig. 4B). Longitudinal sections of the welds revealed that undercutting in the high-current range was accompanied by the formation of discontinuous tunnels at the root of the bead.

Figure 5 shows the maximum dimensions and the cross-sections of the weld beads obtained with various currents at the travel-speed limit. In the current range below 250 A (Range I), the penetration is formed mainly by arc heat and convection of the molten

metal, and the effect of arc force is apparently small. The cross-section at 250 A shows this clearly. The observed concave root is a characteristic sign that the convection is active in the weld pool.[1] If the arc force were influential in the formation of the weld, the root of the bead would have been convex.

The medium-current range (Range II) can be considered to be a transition stage with respect to the effect of arc force on the penetration. By increasing the current within this range, the arc force is increased gradually. This increase in arc force changes the root shape from concave to flat to convex. When the current is increased beyond 430 A (Range III), both the bead width and the penetration depth increase sharply. The abrupt decrease in travel-speed limits shown in Fig. 3 may be related to this phenomenon.

Effect of Electrode-Surface Condition

The effect of the electrode-surface condition, already briefly discussed, is illustrated in Fig. 6. By using an electrode pre-conditioned with a higher current than that used in determining the travel-speed limit, the travel-speed limits are increased above those obtained when the electrodes were pre-conditioned with the same current. This fact emphasizes the importance of the electrode-surface condition.

During this investigation, all other electrodes were pre-conditioned using the current employed to determine the travel-speed limit.

Effect of Shielding Gas

As mentioned earlier, the plasma jet is the most powerful component of the arc pressure. Theoretical analysis[1,8,9] shows that the arc pressure resulting from the plasma jet is independent of the gas density.

In Fig. 7, which compares He and Ar shielding, the curve for He shows much higher travel-speed limits than that for Ar. As an example, the speed limit with He shielding at 400 A exceeds that for Ar shielding by a factor of three. This fact suggests that the arc pressure of the He-shielded arc may be much lower than that of the Ar-shielded arc.

Considering the maximum dimensions and the penetration shapes of the weld beads obtained with He shielding, the penetration shows a concave root in the current range up to 450 A, and at 500 A the root becomes flat. In the case of Ar shielding, the transition current between a concave and a flat root geometry was 250–300 A, as shown previously in Fig. 5. This difference in the penetration shape between He and Ar shielding also suggests that the pressure of the He-shielded arc may be lower than that of the Ar-shielded arc.

According to theoretical analysis,[1,8] the only factor which affects the arc pressure is the electro-magnetic pressure difference between the regions adjacent to the electrode and the plate. This pressure difference is caused by the current-density difference between the two regions. Consequently, when different shielding gases are used, the arc shape changes and this shape difference is considered to be the main cause for the difference in the travel-speed limit. The major feature of the Ar-shielded arc is that a brighter and more slender arc column can be observed in the center of the arc. On the other hand, the He-shielded arc exhibits relatively large anode spots on the rear surface of the molten pool.

Effect of Electrode-to-Work Distance

The electrode-to-work distance is one of the important factors which affect the travel-speed limit. The stiffness of arc, i.e., the arc force against a plate surface, is inversely proportional to the electrode-to-work distance.

Figure 8 shows the effect of the electrode-to-work distance on the travel-speed limit for both Ar and He shielding. The curves indicate that the travel-speed limits for a shorter arc length exceed those for a longer arc length.

The maximum dimensions and the cross-sections of the welds obtained at the travel-speed limits are shown in Fig. 9. As the electrode-to-work distance is increased, the shape of the weld root changes from flat to convex for the Ar shielding, and concave to flat for the He shielding. These trends suggest that the arc pressure at a

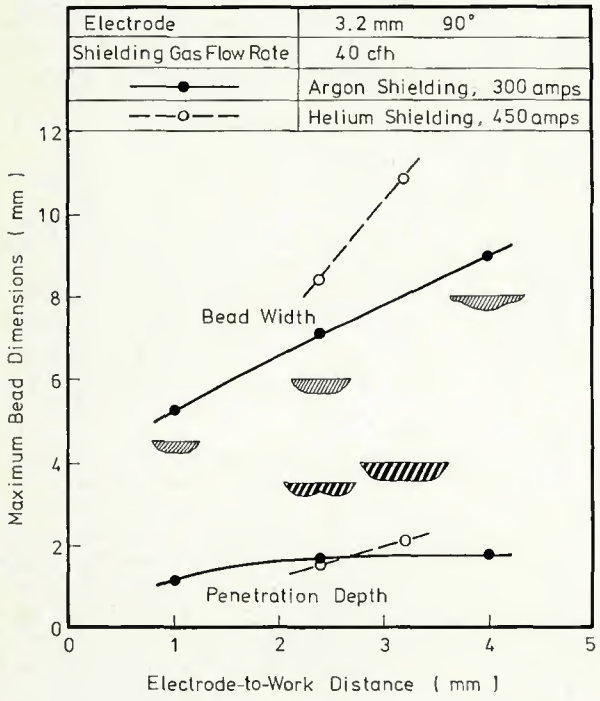

Fig. 9—Maximum dimensions and cross-sections of the weld beads obtained with different shielding gases and different electrode-to-work distances

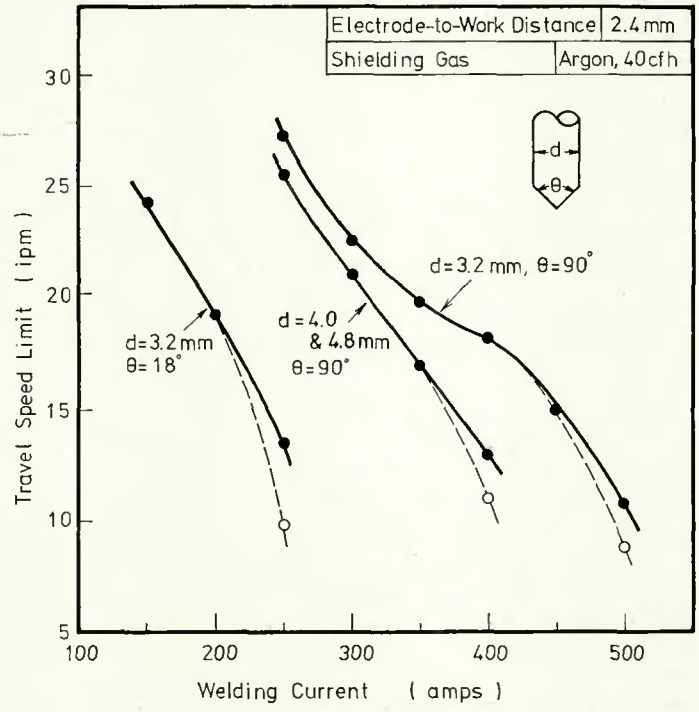

Fig. 10—Effect of electrode geometry on travel-speed limit

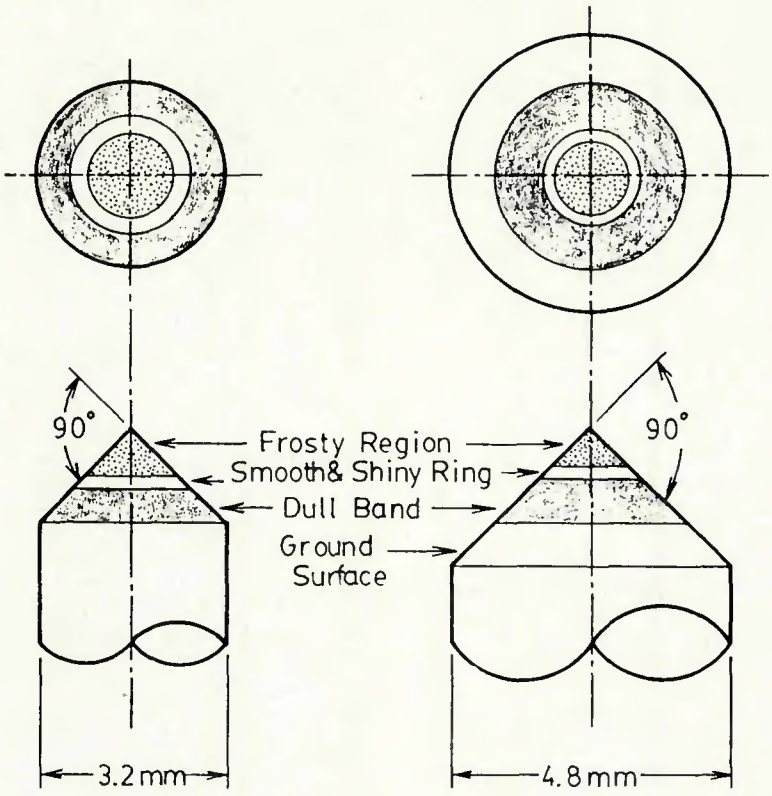

Welding Current : 350 amps
Electrode-to-Work Distance: 3.2 mm
Shielding Gas : Argon, 40 cfh
Arc Time : 10 seconds

Fig. 11—Comparison of the electrode-tip pattern for different diameter electrodes

longer distance may be stronger than that at a shorter one. This is also inconsistent with the expected effect of arc length on arc force.

Effect of Electrode Geometry

Several researchers have indicated that the tip shape of a W electrode exerts a significant influence upon arc phenomena and the weld-bead formation. Savage, *et al.*[11] have shown that, as the vertex angle of the conical tip is decreased within the range from 120 to 30 deg, the effective arc length is increased even if the electrode-to-work distance is held constant. As a result wider and shallower weld beads are formed with smaller vertex angles.

Okada, *et al.*[12] have shown that the plasma-jet pressure beneath the electrode reaches a peak value at a vertex angle of 45 deg, and decreases for both larger and smaller angles. Okada has also reported[13] that the jet pressure can be reduced by using a wedge-shaped tip on the electrode.

Electrodes with three different diameters and two different vertex angles were used to study the effect of electrode geometry on the formation of weld defects. The relationships between the electrode geometry and the travel-speed limit are shown in Fig. 10. For a given electrode diameter, the travel-speed limits are greatly increased by using an electrode with the vertex angle of 90 deg rather than 18 deg. For a given vertex angle, using a smaller diameter electrode increases the travel-speed limit.

From the standpoint of the current density at a conical tip, a thicker electrode is supposed to result in a lower current density and consequently one would expect a higher travel-speed limit. However, the experimental results are directly contrary to this expectation.

To compare the surface conditions of the conical tips of electrodes with different diameters, stationary arcs were operated at 350 A for approximately 10 s using 3.2 and 4.8 mm (⅛ and 3/16 in.) diameter electrodes. Figure 12 shows, in schematic form, the surface appearance of the conical tips after the 10 s arc time. At the extreme point of a conical tip there is a frosty region which is surrounded by a smooth, shiny ring. Outside the shiny ring, a dull, degenerate band extended over the balance of the conical tip of the 3.2 mm (⅛ in.) electrode. On the other hand, the 4.8 mm (3/16 in.) electrode exhibited a region of as-ground surface outside of the degenerate band.

The dimension of the frosty region of the 3.2 mm (⅛ in.) diameter electrode, measured along the conical surface, was 1.12 mm (0.044 in.), which was much larger than the 0.90 mm (0.035 in.) dimension for the 4.8 mm (3/16 in.) electrode. On the assumption that the majority of the welding current flows through the frosty region, the average current density can be calculated as follows: 3.2 mm (⅛ in.) diameter electrode—126 A/mm^2; 4.8 mm (3/16 in.) diameter electrode—195 A/mm^2. Thus, the 4.8 mm (3/16 in.) diameter electrode appears to have experienced a higher current density at its conical tip than did the 3.2 mm (⅛ in.) electrode. The reason for this phenomenon is not clear and should be the subject of future research.

Figure 12 shows the maximum dimensions and the cross-sections of the weld beads obtained with two different electrode geometries. By comparing Fig. 12 with Fig. 5, it may be noted that the electrode which results in the higher travel-speed limits has a tendency to experience a transition from a concave to convex root at a higher current. This fact suggests that the arc force may decrease with a decrease in the electrode diameter and with an increase in the vertex angle.

Effect of Pulsed-Current[14-18]

To reveal the effect of pulsed-current on weld-defect formation, experiments were conducted using low-frequency pulsed-current of up to 4 cps. The average current was held at 300 A, and two combinations of the maximum and the minimum current were used. The ratio of the time at maximum current to the time at minimum current was held constant at 1.0.

The relationship between travel-speed limits and pulse frequency is shown in Fig. 13. The data at zero frequency are those obtained with continuous current. As can be seen, the travel-speed limit decreases with increase in pulse frequency. In all cases, humping occurred in the weld pool during the interval of the maximum current. It is believed that a transient increase in current density accompanies the transition from low to high current and that this causes a

transient increase in arc pressure early in the high-current pulse interval.

Effect of Welding Variables on Arc Force

General Characteristics. Some examples of arc-force data are shown in Fig. 14 together with photographs of the corresponding weld beads. The diameter and the vertex angle of the electrode used were 3.2 mm and 90 deg, respectively. Electrode-to-work distance was held constant at 2.4 mm (0.094 in.). The current and travel speed used in each case are noted at the right-hand side of the figure.

In Fig. 14A, arc force is plotted as a function of location for a welding current of 100 A, a current level which did not produce any defects in the weld bead. The average arc force is 3.8 grams throughout the length of the weld bead. Figure 14B shows similar data obtained with an arc current of 450 A, a current level which produced a humping bead. The number of humps which can be seen in the photograph of the weld does not coincide with the observed fluctuations in arc force, the average of which is 11.7 grams.

In Fig. 14C (the data for 550 A), an abrupt increase in arc force can be observed at point A. At point A, the arc plasma climbed up the electrode, as indicated in the sketch at the right, because of super-heating of the electrode tip. The arc plasma remained in this condition until the electrode tip melted free at point B. The tip of the electrode is visible near the left side of the photograph of the weld bead in Fig. 14C. The average arc forces before and after point A were 15.3 and 18.6 grams, respectively.

Figures 14D and E show arc force as a function of location for welds made with pulsed-current, with maximum and minimum currents of 450 and 150 A, respectively. The pulse frequency was 1.15 cps for 14D, and 3.35 cps for 14E. The maximum and the minimum arc force were 11.3 and 3.1 grams for 14D, and 12.3 and 4.5 grams for 14E, respectively.

The influence of welding speed on the arc force was investigated using a 300-A constant current. Within the travel-speed range investigated, from 9 to 34 ipm (3.38 to 14.5 mm/s), the arc force remained constant, regardless of whether or not humping occurred [the travel-speed limit for these conditions was 22.5 ipm (9.5 mm/s)].

Effect of Welding Current. As shown in Fig. 15, the arc force increases linearly with increase in welding current. The scatter in the data indicates that the precision of measurement was approximately ± 1.4 grams. In all cases, the travel speed used was 15 ipm (6.35 mm/s), the travel-speed limit for a current of 450 A. Regardless of whether or not humping occurred, the line has a constant slope. A least-squares fit of the data yielded the equation $F = 0.026I$, with a coefficient of correlation of 0.99, where F is the force in grams and I is the current in amperes.

As indicated in Fig. 3, the travel-speed limit was found to decrease in a non-linear fashion as the welding current was increased. Although the curve of travel-speed limit vs. arc current shows abrupt changes in slope at 250 and 430 A, no corresponding deviations in slope were observed in the arc-force vs. welding-current relationship. The fact that no deviations from the linear arc-current vs. arc-force relationships were observed at currents where abrupt changes were noted in the slope of the arc-current vs. travel-speed-limit curve indicates that the pressure distribution rather than the total arc force may be the dominant factor in the formation of weld defects.

The changes in the effective arc pressure as a function of welding current can be estimated from the critical pressure head of the molten metal at the travel-speed limit.[4] From

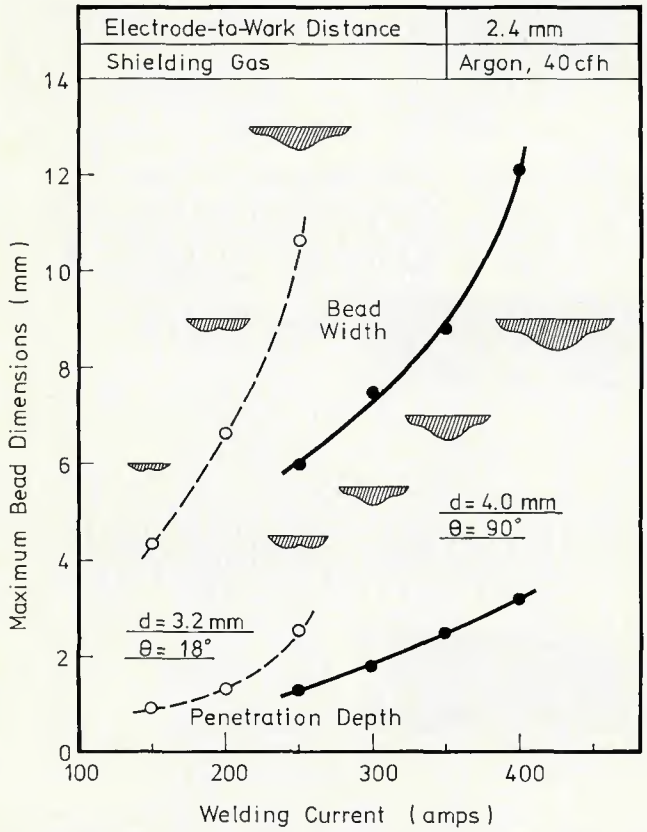

Fig. 12—Maximum dimensions and cross-sections of the weld beads obtained with different electrode geometries

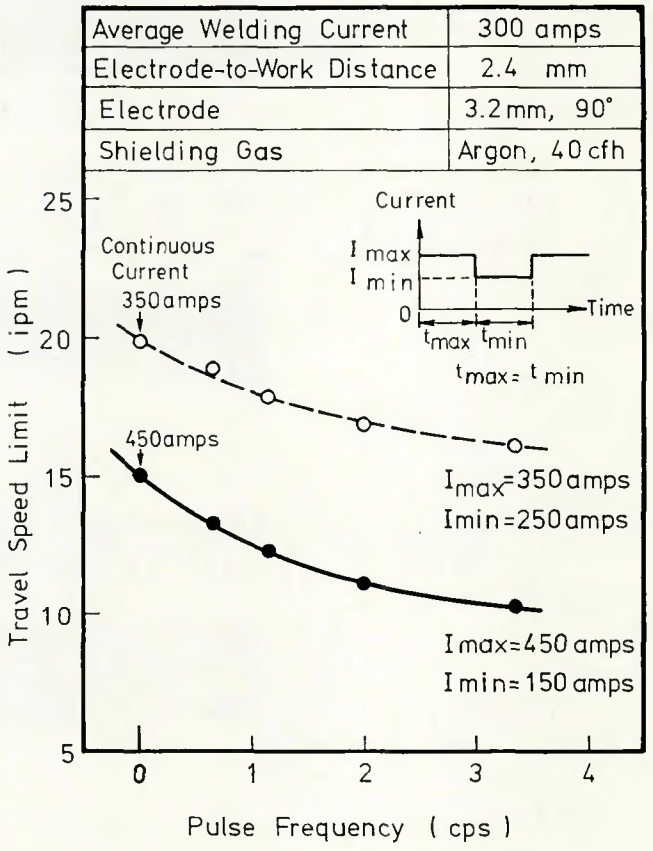

Fig. 13—Effect of pulse frequency on travel-speed limit

Pascal's Laws, $Pa = pgh_1$ where Pa = arc pressure, p = density of the molten metal, g = acceleration due to gravity, and h_1 = critical pressure head of the molten metal. Figure 16 shows the relationship between the pressure head and the welding current. The curve, h_1, represents the height of humps measured from the root of the gouged channel, and the curve, h_2, represents the average depth of the weld metal excluding the areas where humping occurred.

Although the actual head of molten metal during welding cannot be defined by either h_1 or h_2, which were measured from photomacrographs of the solidified welds, this method of estimating both quantities is probably not in error by more than 10%. Because the arc at the travel-speed limit is

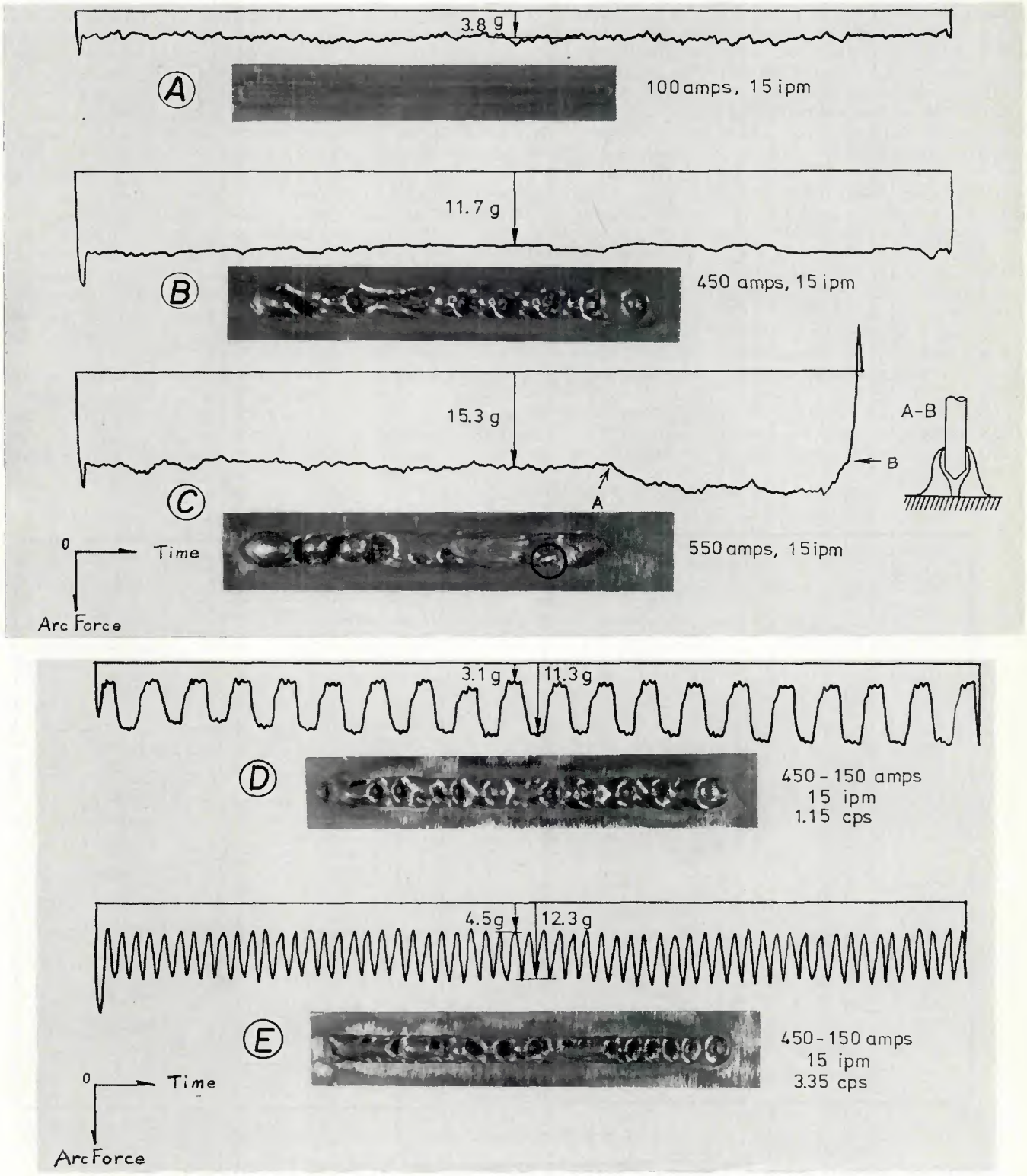

Fig. 14—Arc-force measurements and corresponding bead appearances

believed to operate on solid metal, the effective pressure will be determined by h_1. Thus the effective arc pressure will be defined in terms of estimates of the critical pressure head, h_1, obtained in the above fashion.

As can be seen in Fig 16, the curves h_1 and h_2 show similar trends when plotted as a function of the welding current, with abrupt changes in slope at 250 and 430 A.

Figure 17 shows the relationship between the travel-speed limit and the components of the critical pressure head for the molten metal in the weld pool. In the current range above approximately 250 A, the travel-speed limit decreases linearly as the effective arc pressure is increased. In the current range below 250 A, the travel-speed limit exceeds the value which would be predicted from extrapolation of the linear portions of the effective arc-pressure curves.

In discussing Fig. 5, it was noted that in the lower current range the shape of the weld cross-section suggested that the arc pressure may not be the dominant factor controlling the geometry of the weld. The data shown in Fig. 17 confirm this observation, and it is likely that the surface tension of the molten metal is responsible for the formation of weld defects in the lower current range.

As to the abrupt decrease in the travel-speed limit in the higher current range, it is suggested that an ultra-high velocity gas jet, caused by the evaporation of the electrode material, may be responsible.[19] As evidence for the evaporation of electrode material, it was observed that in the current range above 450 A the ground tip of an electrode acquires a smooth, shiny surface instead of the normal frosty surface indicated in Fig. 11.

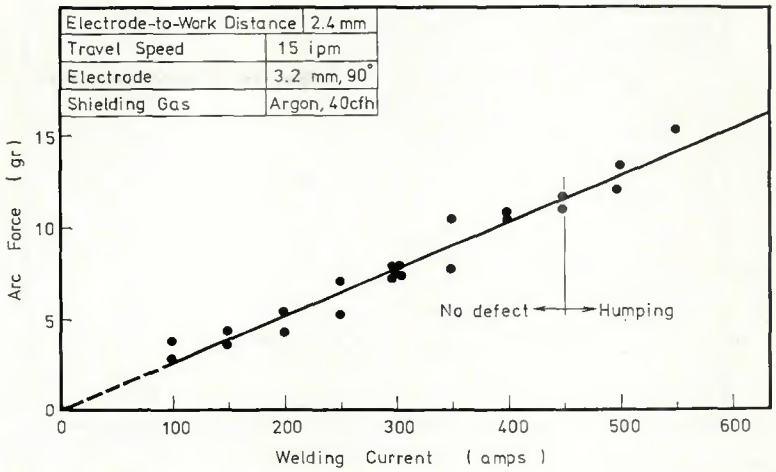

Fig. 15—Effect of welding current on arc force

Effect of Shielding Gas. The travel-speed limit with He shielding was found to be much higher than that with Ar shielding, as shown previously in Fig. 7. On the basis of the penetration geometry, it was speculated that the arc force for the He-shielded arc might be weaker than that for the Ar-shielded arc.

Figure 18 shows the results of the arc-force measurements undertaken to check this speculation. The solid line represents the data presented previously in Fig. 15 for Ar shielding, and the solid circles represent the arc force as a function of welding current with He shielding. As can be seen in Fig. 18, contrary to the original speculation, the arc force is directly proportional to the welding current and is independent of shielding gas.

Thus, in order to explain the difference in the travel-speed limit, it is necessary to consider the effective arc pressure. If, for example, the arc pressure is more uniformly distributed over the surface of the weld pool with a He shield than with an Ar shield, the pressure head of the molten metal

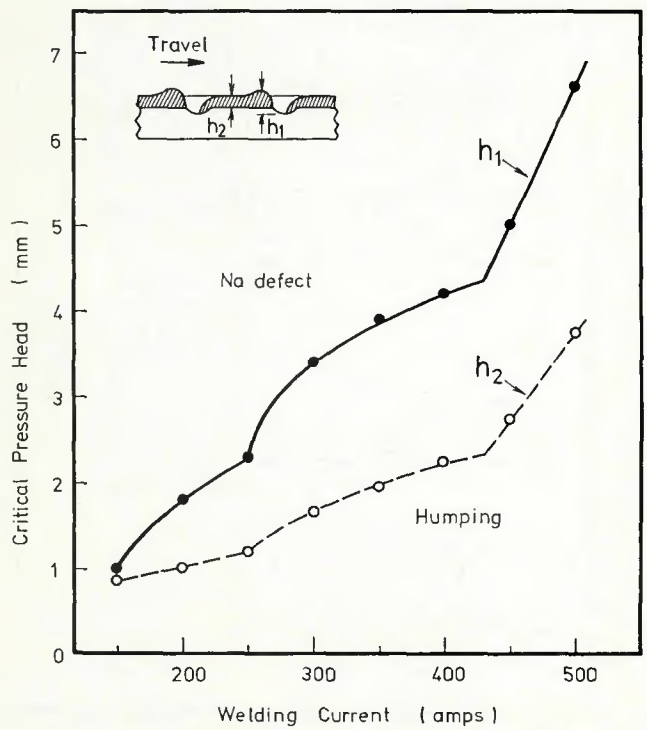

Fig. 16—Effect of welding current on critical pressure head of molten metal

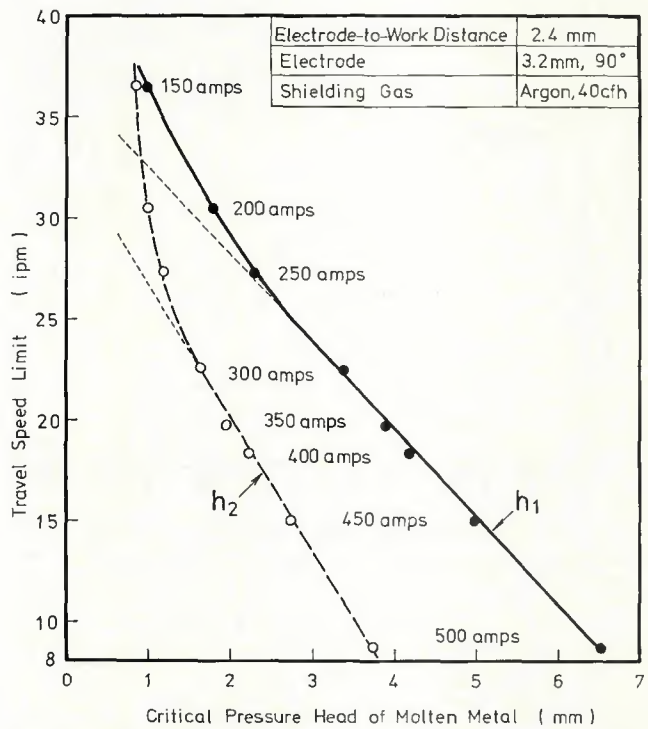

Fig. 17—Relationship between travel-speed limit and critical pressure head of molten metal

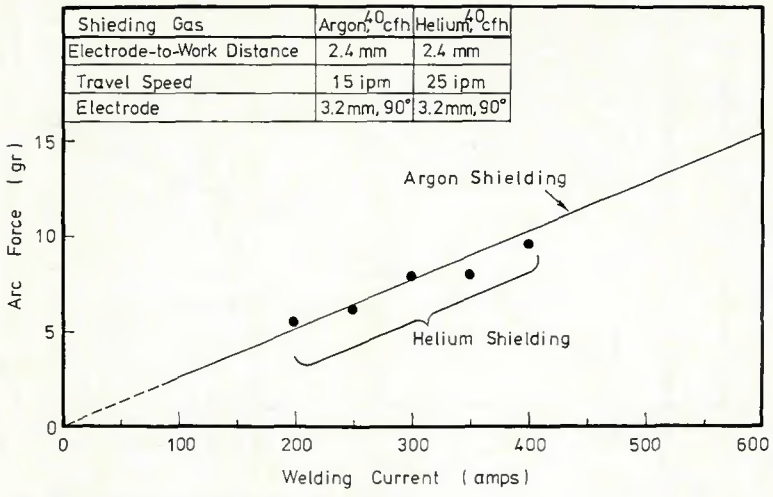

Fig. 18—Effect of shielding gas on arc force

would be reduced. This situation would permit the use of higher welding speeds. Unfortunately, only the total arc force could be measured by the techniques used in this investigation. Possibly high-speed motion pictures of the weld-pool surface might shed additional information on the pressure distribution.

Effect of Electrode-to-Work Distance. The data summarized in Fig. 8 indicated that as the electrode-to-work distance is increased, the travel-speed limit is decreased, in spite of the fact that the arc force would be expected to be diminished by increasing the arc length.

Figure 19 shows the actual relationship between the arc force and the electrode-to-work distance. As might be expected, as the distance is increased, the arc force is decreased. Thus, it is again impossible to explain the variation in the travel-speed limit on the basis of the arc force. This supports the earlier postulation that the effective pressure rather than the total force may govern the travel-speed limit.

Effect of Electrode Geometry. The influence of the electrode geometry on the travel-speed limit was shown in Fig. 10, and it was postulated that the electrode geometry should influence the arc force.

The effect of the vertex angle of a conical tip and the electrode diameter on the arc force were investigated using welding currents which were observed to produce a large difference in the travel-speed limit. A current of 300 A was used for the vertex-angle study (18 vs. 90 deg) and a current of 400 A was used for the electrode-diameter study (3.2 vs. 4.8 mm, 1/8 vs. 3/16 in.). In contrast to the expected behavior, the arc force was found to be independent of both the vertex angle and the electrode diameter. This fact confirms the necessity of considering how the arc-pressure distribution influences the effective arc pressure for the formation of weld defects.

Effect of Pulsed-Current. The relationship between the travel-speed limit and the pulse frequency was reported in Fig. 13. The decrease in travel-speed limit with an increase in pulse frequency was postulated to be a result of the transient arc pressure variation at the transition from low to high current.

Figure 20 shows the arc-force curves measured at a travel speed of 15 ipm (6.35 mm/s). Regardless of the pulse frequency, both the maximum and the minimum arc force show values characteristic of the instantaneous current. Although no transient arc-force changes could be observed (Figs. 14 D

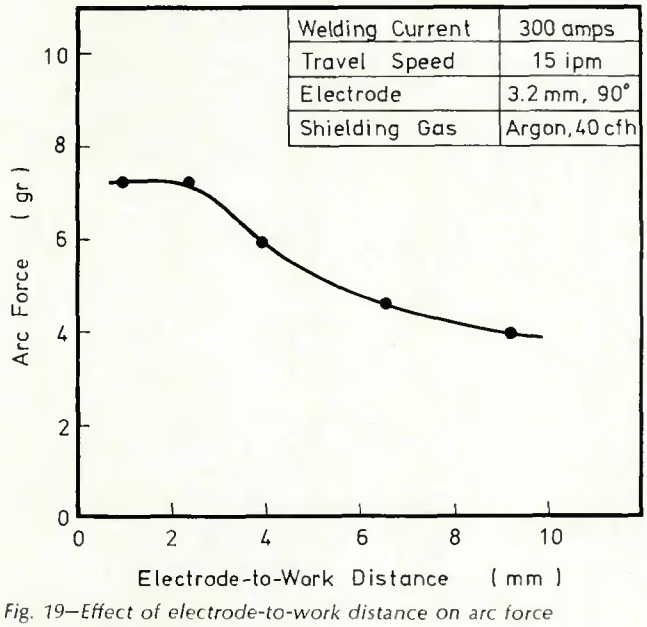

Fig. 19—Effect of electrode-to-work distance on arc force

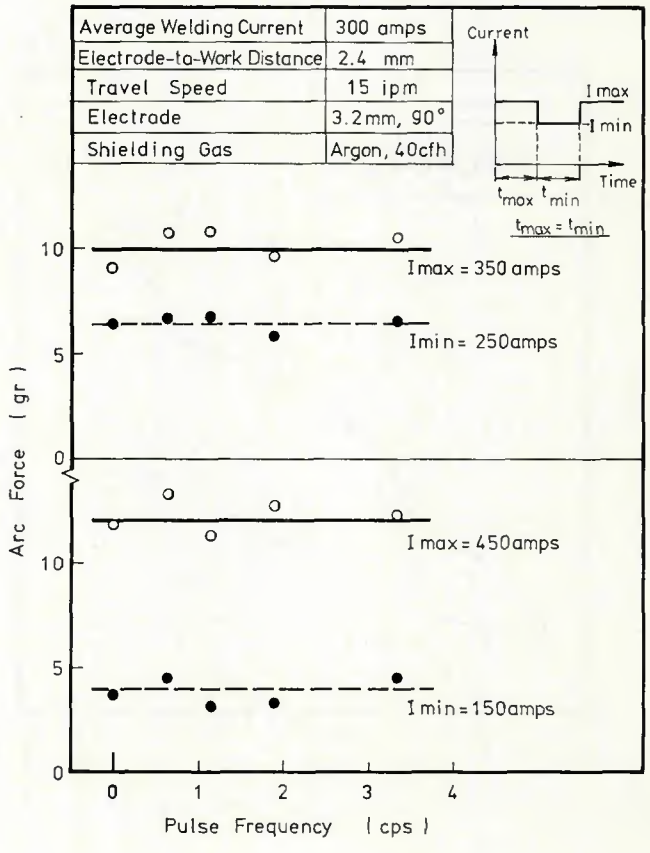

Fig. 20(right)—Effect of pulse frequency on arc force

and E), the frequency response of the arc-force measuring system is too low to detect such transients.

Figure 21 shows the maximum bead dimensions measured at the gouged area of the humped beads. Both the penetration depth and the bead width decrease with increase in pulse frequency. This may be a result of the fact that the time constant for melting approaches the length of the pulse period as the pulse frequency is increased. The transient variation of the pool shape during each pulse may also contribute to the formation of weld defects.

Conclusion

The effect of arc force on the travel-speed limit of GTA welding has been investigated and the following conclusions may be drawn:

1. An effective apparatus was designed and constructed for measuring the total arc force which acts against the plate surface during welding.

2. The arc force is a function of both the welding current and the electrode-to-work distance and is not affected by travel speed, shielding gas, electrode diameter, vertex angle of a conical electrode tip, or pulse frequency.

3. When the electrode-to-work distance is held constant at 2.4 mm, the arc force increases from 2.6 to 14.3 grams when the welding current is increased from 100 to 550 A. A least-squares fit of the data gives the relationship $F = 0.026I$ with a correlation coefficient of 0.99, where F is the total arc force in grams and I is the welding current in amperes.

4. The electrode-surface condition affects the travel-speed limit. Conditioning the electrodes by repeated arc-on intervals at the desired welding current increases the travel-speed limit.

5. There are three current ranges which produce different characteristic relationships between the arc current and the travel-speed limit:

(a) In the current range below 250 A, the travel-speed limit corresponds to the beginning of undercutting, and higher speeds are required to cause humping.

(b) From 250 to 400 A, the travel-speed limit corresponds to the onset of humping, and undercutting is not observed.

(c) Above 400–430 A the travel-speed limit again corresponds to the beginning of undercutting, and higher speeds are required to cause humping.

6. No direct relationship was observed between the travel-speed limit and the arc force. The arc force increases linearly with increase in welding current, while the travel-speed limit decreases gradually up to 400 A and then falls steeply.

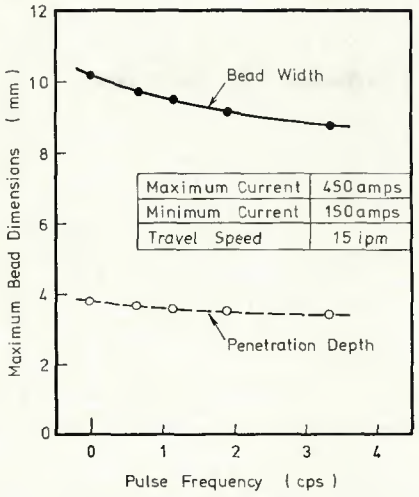

Fig. 21—Maximum dimensions of weld beads obtained with pulsed-current

7. Above 400 A the undercut weld beads also exhibit tunneling at the root.

8. Assuming the humping height at the travel-speed limit as the critical pressure head of the molten metal during welding, the effective arc pressure for the defect formation was estimated on the basis of Pascal's Law. In the current range above 250 A, the travel-speed limit decreases linearly as the effective arc pressure increases, while in the current range below 250 A the travel-speed limit lies at higher speeds above the extrapolated linear portion of the effective-pressure plot. This fact indicates that the effect of the arc pressure is dominant for the formation of weld beads only in the current range above 250 A. Below 250 A, it is postulated that the surface tension is the dominant factor causing weld defects.

9. When the welding current is held constant, the travel-speed limit with a shorter electrode-to-work distance is higher than that with a longer one, despite the higher arc force of the shorter arc.

10. When the electrode-to-work distance is held constant, the travel-speed limit with He shielding is much higher than that with Ar shielding. However, no difference can be observed in the arc force as a result of changing from one shielding gas to the other.

11. When the electrode-to-work distance is held constant, the travel-speed limit is increased by a decrease in the electrode diameter and by an increase in the vertex angle of the conical tip.

12. The total arc force is independent of both the electrode diameter and the vertex angle of the conical tip.

13. At an arc current of 350 A, the current density was decreased by decreasing the electrode diameter from 4.8 to 3.2 mm (3/16 to 1/8 in.).

14. When the electrode-to-work distance is held constant with pulsed-GTA, the travel-speed limit decreases with increase in pulse frequency.

15. The instantaneous arc force during pulsed-GTA welding is determined by the instantaneous current.

16. In all cases, the welding conditions which increase travel-speed limits have a tendency to produce concave or flat root geometries more easily. From this fact, the effective arc pressure for the formation of weld defects is considered to be low under these welding conditions, even though the total arc force remains unchanged.

Acknowledgments

The authors wish to thank the Republic Steel Corporation for supplying the steel used in this investigation and to express their appreciation and thanks to the Kawasaki Steel Corporation for providing financial support.

References

1. Ando, K., and Hasegawa, M., *Welding Arc Phenomena*, Sangyo Pub. Co., 1968 (in Japanese).

2. Nishiguchi, K., and Matsunawa, A., "Gas Metal Arc Welding in High Pressure Atmosphere," *Abstracts of the Second International Symposium of JWS*, Paper No. 2-2-S, August 1975.

3. Yamamoto, T., and Shimada, W., "A Study on Bead Formation in High Speed TIG Arc Welding at Low Gas Pressure," *Ibid.*, Paper No. 2-2-7, August 1975.

4. Paton, B. E., Mandel'berg, S. L., and Sidorenco, B. G., "Certain Special Features of the Formation of Welds Made at High Speeds," *Avt. Svarka*, Vol. 24, No. 8, pp. 1-6, 1971.

5. Nishiguchi, K., Oji, T., and Nakamura, T., "Studies on Weld Defect Formation at High Speeds (Report 3)," *Preprints of the National Meeting of JWS*, No. 20, Paper No. 154, Spring 1977 (in Japanese).

6. Uchida, A., "Arc Force Measurement in Argon Atmospheres," *Journal of the JWS*, Vol. 29, p. 453, 1960 (in Japanese).

7. Needham, J. C., Cooksey, C. J., and Milner, D. R., "Metal Transfer in Inert-Gas Shielded-Arc Welding," *British Welding Journal*, Vol. 7, p. 101, 1960.

8. Greene, W. J., "An Analysis of Transfer in Gas Shielded Welding Arcs," *A.I.E.E. Winter General Meeting*, 1960.

9. Wilkinson, J. B., and Milner, D. R., "Heat Transfer from Arcs," *British Welding Journal*, Vol. 7, pp. 115-128, February 1960.

10. Koizumi, I., Yamauchi, N., and Koh, T., "Studies on Gas Tungsten-Arc Welding Process," *Preprints of the National Meeting of JWS*, No. 20, Paper No. 213, Spring 1977 (in Japanese).

11. Savage, W. F., Strunck, S. S., and Ishikawa, Y., "The Effect of Electrode Geometry in Gas Tungsten-Arc Welding," *Welding Journal*, 44 (11), Nov. 1965,

Research Suppl., pp. 489-s to 496-s.

12. Okada, A., Hiraoka, K., and Inagaki, M., "The Effect of Electrode Geometry on the Arc Pressure in GTA Welding," *Preprints of the National Meeting of JWS*, No. 18, Paper No. 214, Spring 1976 (in Japanese).

13. Okada, A., "Control of the Weld Bead Formation with Inert-Gas Jet," *Preprints of the National Meeting of JWS*, No. 20, Paper No. 226, Spring 1977 (in Japanese).

14. Shimada, W., *et al.*, "Characteristics of the High-Frequency Pulsed-GTA Welding," *Preprints of the National Meeting of JWS*, No. 17, Paper No. 449, Fall 1975 (in Japanese).

15. Petrov, A. V., and Birman, U. I., "Method of Studying Weld Metal Crystallization During Pulsed Arc Welding," *Svar. Proiz.*, Vol. 14, No. 10, pp. 27-29, 1967.

16. Vagner, F. A., and Stepanov, V. V., "Choice of Welding Settings for Pulsed Arc Welding and Its Effect of Joint Properties," *Ibid.*, Vol. 15. No. 5, pp. 14-16, 1968.

17. Petrov, A. V., and Birman, V. I., "Solidification of Weld Metal in Pulsed Arc Welding," *Ibid.*, Vol. 15, No. 6, pp. 1-3, 1968.

18. Shnaider, B. I., and Rossoshinskii, A. A., "The Melting and Solidification of Pulsed Arc Spot Welds," *Avt. Svarka*, Vol. 20, No. 3, pp. 23-25, 1967.

19. Weinecke, R., "Uber das Auftreten von Dampfstrahlen in Kohlenlichitbogen Hocher Stromstärken," *Z. Phys.*, Vol. 150, p. 231, 1958—Vol. 151, p. 159, 1959.